Experimental Neurology 314 (2019) 20–33

Contents lists available at ScienceDirect

Experimental Neurology

journal homepage: www.elsevier.com/locate/yexnr

Research Paper

EPPS treatment attenuates traumatic brain injury in mice by reducing Aβ burden and ameliorating neuronal autophagic flux

Angela Melinda A. Anthony Jalin, Rong Jin, Min Wang, Guohong Li*

Department of Neurosurgery, Neuroscience Institute, Penn State Hershey Medical Center, Hershey 17033, USA

ARTICLE INFO

Keywords:
Traumatic brain injury
Neuroprotection
Axonal injury
Beta-amyloid
Autophagy

ABSTRACT

Beta-amyloid (Aβ) burden and impaired neuronal autophagy contribute to secondary brain injury after traumatic brain injury (TBI). 4-(2-hydroxyethyl)-1-piperazinepropanesulphonic acid (EPPS) treatment has been reported to reduce Aβ aggregation and rescue behavioral deficits in Alzheimer's disease-like mice. Here, we investigated neuroprotective effects of EPPS in a mouse model of TBI. Mice subjected to controlled cortical impact (CCI) were treated with EPPS (120 mg/kg, orally) immediately after CCI and thereafter once daily for 3 or 7 days. We found that EPPS treatment profoundly reduced the accumulation of beta-amyloid precursor protein (β-APP) and Aβ over a widespread area detected in the pericontusional cortex, external capsule (EC), and hippocampal CA1 and CA3 at 3 days after TBI, accompanied by significant reduction in the TBI-induced diffuse axonal injury identified by increased immunoreactivity of SMI-32 (an indicator for axonal damage). We also found that EPPS treatment ameliorated the TBI-induced synaptic damage (as reflected by enhanced postsynaptic density 95, PSD-95), and impairment of autophagy flux in the neurons as reflected by reduced autophagy markers (LC3-II/LC3-I ratio and p62/SQSTM1) and increased lysosomal enzyme cathepsin D (CTSD) in neurons detected in the cortex and hippocampal CA1. As a result, EPPS treatment significantly reduced the TBI-induced early neuronal apoptosis (assessed by active caspase-3), and eventually prevented cortical tissue loss and hippocampal neuronal loss at 28 days after TBI. Additionally, we found that inhibition of autophagic flux with chloroquine by decreasing autophagosome-lysosome fusion significantly reversed the decreased expressions of neuronal p62/SQSTM1 and apoptosis by EPPS treatment. These data suggest that the neuroprotection by EPPS is, at least in part, related to improved autophagy flux. Finally, we found that EPPS treatment significantly improved the cortex-dependent motor and hippocampal-dependent cognitive deficits associated with TBI. Taken together, these findings support the further investigation of EPPS as a treatment for TBI.

1. Introduction

Traumatic brain injury (TBI) is a critical public health and socio-economic problem throughout the world, with > 1.7 million TBI cases reported annually in the United States (Faul et al., 2010; Roozenbeek et al., 2013). Primary brain injury that occurs at the moment of impact and involves immediate neuronal axonal damage, is irreversible. Secondary injury of TBI is a prolonged but reversible pathogenic process leading to further neurological injury mediated by complex mechanisms such as excitotoxicity, oxidative stress, apoptosis, inflammatory events, and mitochondrial dysfunction (Algattas and Huang, 2013). Secondary injury can thus be attenuated or prevented by appropriate medical intervention. However, effective neuroprotective therapy for clinical TBI remains limited, due in part, to the pathological complexity of human TBI.

Secondary axonal injury appears to be the most prominent and sustained pathological feature of all types of TBI in human and animals, ranging from mild to severe (Laskowski et al., 2015). Studies have linked the propagation of axonal injury with the impairments of cortex-dependent motor and hippocampus-dependent cognitive functions across the spectrum of TBI severity (Kumar et al., 2009). Degenerated axon enhances the production of beta-amyloid precursor protein (β-APP) as a sign of complete axonal disconnection (Reichard et al., 2005). The sites of β-APP accumulation then serves as reservoirs for neurotoxic Aβ formation which can further exacerbate neuronal death and behavioral dysfunction following TBI (Mondello et al., 2014; Scott et al., 2016). Furthermore, TBI survivors with prolonged Aβ amyloidosis have higher risks of developing other neurodegenerative disorders at later

* Corresponding author.
E-mail addresses: aanthonyjalin@pennstatehealth.psu.edu (A.M.A. Anthony Jalin), rjin@pennstatehealth.psu.edu (R. Jin), mwang2@pennstatehealth.psu.edu (M. Wang), guohongli@pennstatehealth.psu.edu (G. Li).

https://doi.org/10.1016/j.expneurol.2019.01.002
Received 12 September 2018; Received in revised form 2 January 2019; Accepted 3 January 2019
Available online 09 January 2019
0014-4886/

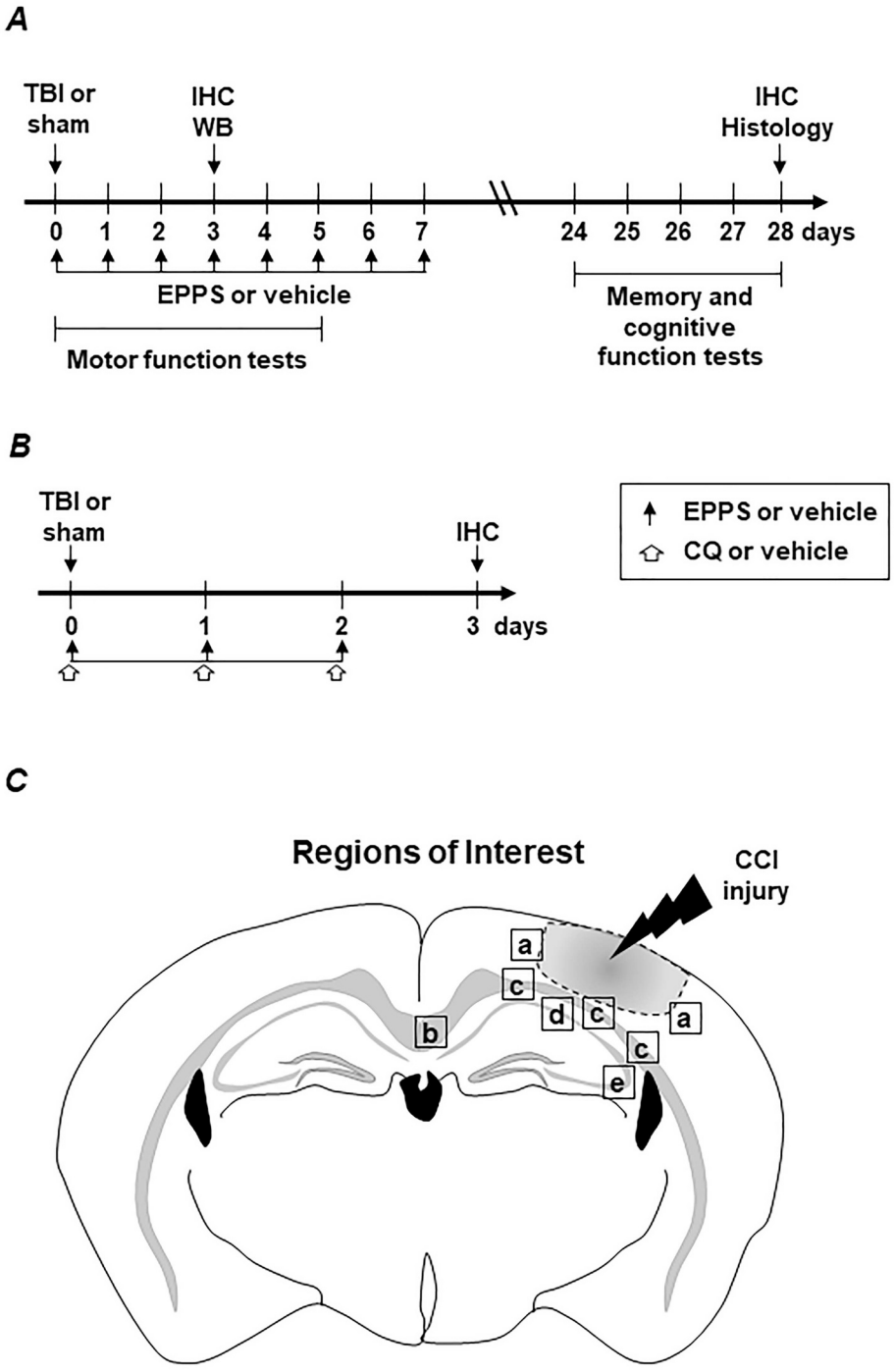

Fig. 1. (A) Schematic diagram describing the experimental design. IHC, immunohistochemistry; WB, western blot. (B) Experimental design showing the administration of EPPS (120 mg/kg) and/or chloroquine (CQ, 10 mg/kg) or vehicle. (C) Schematic diagram showing the regions of interest (ROI) selected for immunohistochemical image acquisition and quantitative analysis: from the cortex (a), corpus callosum (b), external capsule (c), hippocampal CA1 (d) and CA3 (e).

stage such as Alzheimer's disease (AD) (LoBue et al., 2017).

It is well-acknowledged that neuronal cell death following TBI occurs critically as a result of secondary injuries. Recently, autophagic neuronal cell death has received increasing attention in defining secondary injury mechanisms of TBI. Although autophagy has been associated with both cell survival and cell death, the role of autophagy in neurodegenerative disorders remains controversial. Basal autophagy in normal condition controls cell homeostasis by removing damaged organelles and toxic macromolecules, which appears to be essential for normal cellular function and survival especially in terminally differentiated cells, such as neurons. It is over-activated under stress and disease conditions in attempting to restore homeostasis (Banerjee et al., 2010). It has been suggested that impairment of autophagic flux, a cascade that remove cargo-containing autophagosome by lysosome, rather than autophagy activation per se, could be the main perpetrator of autophagy-related cytotoxicity in the central nervous system (CNS) (Button and Luo, 2017; Piras et al., 2016). The impairment of autophagic flux is often characterized by excessive accumulations of autophagic proteins, microtubule-associated protein 1 light chain 3 (LC3) and p62/SQSTM1 (sequestosome 1), which are evidently detected following TBI in humans and animals, and are associated with dysfunction of lysosomal enzymes such as cathepsin D (CTSD), leading to decreased

autophagosome clearance (Au et al., 2017; Liu et al., 2008; Sarkar et al., 2014).

4-(2-hydroxyethyl)-1-piperazinepropanesulphonic acid (EPPS, also known as HEPPS) is a buffering agent commonly used in biological research. Kim et al. recently reported that EPPS can selectively bind and convert cytotoxic Aβ fibrils and oligomers into non-toxic monomers (Kim et al., 2015). They also found the neuroprotective effects of EPPS in amyloid precursor protein (APP) and presenilin 1 (PS1) double transgenic mice, an animal model for AD, where oral administration of EPPS reduced brain Aβ plaque deposition and neuroinflammation, thus reduced cognitive deficits. As Aβ burden plays a fundamental role in deteriorating the neurological functions following TBI, treatment with EPPS could be beneficial in treating TBI. In the present study, we investigated the therapeutic effects of EPPS in a mouse model of TBI by examining axonal injury, autophagy-mediated neuronal death, and neurological functional outcomes.

2. Materials and methods

2.1. Mice

Male C57BL/6 J mice (8 to 10 weeks old) purchased from Jackson Laboratories (Bar Harbor, ME) were maintained on a 12-h light/dark cycle with ad libitum access to food and water. All mice were acclimated to environment for a week before use. All experimental protocols were approved by Institutional Animal Care and Use Committees (IACUC) at Louisiana State University Health Sciences Center Shreveport and Pennsylvania State University Hershey Medical Center. A total of 92 mice were used in this study. Number of animals used in each experimental measurement is elaborated in more detail in Suppl. Table I.

2.2. Controlled cortical impact (CCI) injury model

Traumatic brain injury (TBI) was induced using a computer-controlled cortical impact (CCI) device (PinPoint Precision Cortical Impactor, Hattera, PCI 3000), as previously described (Bilgen, 2005). Mice were anesthetized with intraperitoneal injection of ketamine (80 mg/kg) /xylazine (5 mg/kg) and placed in a stereotaxic frame (David Kopf Instruments, Tujunga, CA, USA). A midline sagittal scalp incision is made to expose the skull bone. A 4-mm craniotomy was made by using an electric drill on the right lateral side of the skull centered 2.7 mm lateral from the midline and 2 mm posterior to bregma, leaving the dura mater intact. Then, an impactor tip (3 mm in diameter) was placed in the center of the craniotomy site. The impact was then delivered at following parameters: 2 mm depth, 2 m/s velocity, and 85 ms dwell time. These parameters produce *moderate-to-severe* TBI injury in mice as documented previously (Siebold et al., 2018). After impact, Surgicel (Johnson & Johnson, Dallas, TX) was applied to the dura, the skull-cap was then replaced and affixed with dental adhesive, and the incision was closed. Rectal temperature was maintained at 37 ± 0.5 °C with a feedback-regulated heating pad throughout the surgical procedure until the mice recovered from anesthesia. Sham-operated mice underwent the same procedure without impact.

2.3. Experimental design and drug treatment

Schematic diagram for the experimental design is shown in Fig. 1A. Mice were randomly assigned to the following experimental groups before surgery: (1) sham, (2) TBI + vehicle, and (3) TBI + EPPS, and sacrificed at 3 days or 28 days after surgery. For randomization, the web tool www.randomizer.org was used. Animals were randomly assigned to each group via random numbers generated on an Excel spreadsheet. EPPS (Sigma, St. Louis, MO) was freshly dissolved in distilled water with a final concentration of 30 mg/ml. EPPS was administered orally at a dose of 120 mg/kg given immediately after TBI and thereafter once daily for up to 3 days (for the 3-day post-TBI assessment) or 7 days (for 28-day post-TBI assessment). Mice in sham and vehicle groups received the same volume of distilled water. In a separate set of experiments (Fig. 1B), we evaluated the inhibition of autophagic flux on TBI-induced Aβ deposition and neuronal apoptosis at 3 days after surgery, in which the lysosomal inhibitor, chloroquine (CQ), was injected (Sigma, dissolved in saline solution) intraperitoneally at 10 mg/kg prior to EPPS treatment and the assessments were performed in the following experimental groups: (1) sham, (2) TBI + vehicle, (3) TBI + CQ, (4) TBI + EPPS, and (5) TBI + EPPS + CQ.

2.4. Motor function assessment

All functional tests were performed by investigators blinded to group assignment. Motor balance and coordination were assessed using a beam-walk and beam-balance tasks as described previously (Luong et al., 2011). In the beam-walk task, mice were trained and assessed using a negative reinforcement paradigm to escape ambient light and high decibel noise by walking across an elevated (50 cm) narrow wooden beam (6 mm in width × 100 cm in length) and entering into a darkened goal box at the opposite end. Latency to walk across the beam were recorded. In the beam-balance task, mice were placed on the same elevated narrow wooden beam and the duration of the mice remain on the beam were recorded (maximum time was 60 s). All mice were pre-trained on beam-walking and beam-balance 1 day before TBI and assessed right before TBI to establish a basal level of performance. Post-operative testing was conducted at 1 day after TBI and for five consecutive days, consisting of three trials per day for each animal with 60 s allotted time per trial. The average daily scores for each animal were used for statistical analysis.

2.5. Cognitive function assessment

To evaluate the spatial learning and memory function, the Barnes maze test was performed as described previously (Patil et al., 2009). In brief, a small dark recessed chamber (called as target box) was placed under a circular platform (91 cm of diameter) where mice can access it through an escape tunnel under the target hole. Mice were pre-trained with the use of the escape tunnel at 23 days after surgery, and then went through 4 trials per day with a 15 min inter-trial interval for 5 days. During each trial, the mice were placed in the center of the maze under a start chamber for 10 s with both the buzzer (85 dB) and light on (80-watts bulb; 90 cm above maze) to motivate the mice to find the target box and allowed to explore the maze for 3 min. The time spent to reach the target hole was recorded. Data from 4 trials per day for each animal were averaged. Then, they were required to remain in the target box for 2 min prior to retrieval, regardless of success. On the last day, a single trial lasting for 3 min was performed with the target box removed, and mice were allowed to explore the maze and locate the target hole. Number of error head pokes was recorded.

Novel object recognition test was also performed for cognitive assessment as previously described (Leger et al., 2013). At 28 days after TBI, mice were placed in a rectangular arena (30 cm × 30 cm). In the first session (Session 1), mice were allowed to explore two identical objects for 10 min and then returned to their home cages. One hour later (Session 2), mice were exposed to a familiar object from Session 1 and a novel object (same dimension but different in shape and colour) for 10 min. The time spent in exploring each object in Session 2 was recorded. The mouse directing its nose within 2 cm distance to the object, or sniffing or pawing the object was defined as object exploration. The data was expressed as discrimination index using following formula: Discrimination index = time spent in exploring novel object / (time exploring novel object + time exploring familiar object) x 100%.

2.6. Tissue processing

At the indicated time points after TBI, mice were euthanized by *intraperitoneal injection* of sodium *pentobarbital* (Nembutal, 150 mg/kg) and transcardially perfused with 0.01 M phosphate buffered saline (PBS, pH 7.4), followed by 4% paraformaldehyde (PFA, Sigma) in PBS (pH 7.4). Then, the brains were removed, post-fixed overnight in 4% PFA. To prepare frozen sections, brains were transferred into 30% sucrose solution until they sank to the bottom of the container. Then, the brains were frozen-embedded in optimal cutting temperature (OCT) compound (Tissue-Tek, Sakura, Torrance, CA). Coronal sections (8-μm thick) were serially cut using a cryostat, and mounted on silane-coated glass slides (Electron Microscopy Science, Hatfield, PA) and stored at −80 °C. To prepare paraffin sections, post-fixed brains were embedded in paraffin. Coronal sections (5-μm thick) were serially cut using a rotary microtome (Thermo Fisher Scientific, Waltham, MA) and mounted on gelatin-coated glass slides (Frosted, Fisher).

2.7. Contusion volume measurement

Contusion volumes were measured at 28 days after CCI by an investigator blinded to the animal groups. Coronal paraffin sections (5-μm thick) at 0.5 mm intervals were stained using Hematoxylin and Eosin (H&E) staining. Whole coronal section images were acquired using tiling mode and 10× objective on a digital camera system connected to a Nikon Eclipse Ti bright field microscope (Tokyo, Japan). The area of cortical tissue loss for each section was measured on the digital photographs using NIH ImageJ software (Version 1.51n, NIH, Bethesda, MD). Contusion volume (V, mm^3) was calculated based on the contused area (A, mm^2) on 15 coronal sections at 500 μm distance (d = 0.5 mm between two sequential slices) using the following formula: $V = d \times (A1 \times 0.5 + A2 + A3 + \ldots + A14 + A15 \times 0.5)$, as described previously (Dash et al., 2010).

2.8. Hippocampal neuronal loss measurement

Hippocampal neuronal loss induced by TBI was assessed at 28 days after CCI by an investigator blinded to the group assignment. H&E staining was performed on serial paraffin sections at the level of the dorsal hippocampus (−1.4 to −2.1 mm from bregma) at 100-μm intervals. To maintain consistency across animals, four rectangular boxes (1.0 × 0.25 mm) were centered over the CA1 and CA3 layer. CA1 and CA3 pyramidal neurons showing intact round nuclei were counted as surviving cells using a Nikon Ti-E light microscope at 40× magnification. The data are expressed as the number of surviving neurons per millimeter of medial CA1 or CA3 as described previously (Choi et al., 2005).

2.9. White matter damage measurement

Luxol Fast Blue (LFB) staining, a well-established method to stain myelin/myelinated axon, was performed to evaluate white matter damage at 28 days after CCI. A NovaUltraTM LFB stain kit (IHC World, Ellicott City, MD) was used according to the manufacturer's instructions. Images were taken with a 40× objective and LFB intensity was measured using Image-Pro Premier 3D software version 9.2 (Media Cybernetics, Rockville, MD). The average intensities of the regions of interest (ROI) from the external capsule (EC) were used for data analysis (Fig. 1C). All measurements were performed in a blinded manner.

2.10. Immunohistochemistry

Coronal paraffin sections (5 μm thick) from the center of the lesions (−1.5 mm to −2 mm from bregma) were used for immunohistochemistry. The following primary antibodies were used: rabbit anti- β-APP (1:200; Thermo Fisher Scientific, 51–2700), rabbit anti-Aβ (1:200; Abcam, ab2539), mouse anti-nonphosphorylated neurofilament-H (SMI-32; 1:1000; Millipore, NE1023), rabbit anti-p62/SQSTM1 (sequestosome 1; 1:200; Abcam, ab91526), mouse anti-cathepsin D (CTSD; 1:200; Santa Cruz Biotechnology, sc-377,299), rabbit anti-NeuN (neuronal marker; 1:500; Abcam, ab177487), mouse anti-NeuN (1:300; Millipore, MAB377), and rabbit anti-activate caspase-3 (A. casp-3; 1:100; Millipore, AB3623). Isotypes matched control antibodies served as negative controls. For double immunofluorescence staining, the corresponding fluorochrome-conjugated secondary antibodies were used: goat anti-rabbit Alexa Fluor 488 with goat anti-mouse Alexa Fluor 555, and goat anti-mouse Alexa Fluor 488 with goat anti-rabbit Alexa Fluor 555 (all from Life Technology, 1:1000). All images were taken under a 40× magnification using a fluorescence Nikon Ti inverted microscope (Tokyo, Japan). Fluorescence intensities were measured using ImageJ software by applying global background subtraction and threshold adjustment as described previously (Jensen, 2013). The number of immunoreactive cells were counted in predefined areas and expressed as mean cell number/0.1 mm^2. Numbers of positively-stained target cells and intensities of positively-stained areas per mm^2 were analyzed on 5 coronal sections of each brain within the regions of interest (Fig. 1C): the pericontusional cortex, the external capsule (EC), and the hippocampal CA1 and CA3 subfields. All data were analyzed in a blinded manner.

2.11. Western blot analysis

Whole-cell protein extracts were obtained from the ipsilateral cerebral cortices (+1 to −4 mm from bregma). Brain tissues were homogenized in cold RIPA buffer (50 mM Tris-HCl with pH 8.0, 150 mM NaCl, 0.5% sodium deoxycholate, 0.1% SDS, 1 mM EDTA, 1% NP-40) containing protease inhibitor (Pierce tablet; Thermo Fisher Scientific, A32965) and phosphatase inhibitor (Sigma, P0044). The homogenates were centrifuged at 13,000 rpm for 20 min at 4 °C, and the supernatants were used for analysis. Protein content was measured using Bradford dye reagent (Bio-Rad, Hercules, CA). Protein samples (30 μg protein per sample) were separated by 4–20% gradient SDS-PAGE (Invitrogen) and transferred to PVDF membranes. The following primary antibodies were used: rabbit anti-LC3B (1:2000; Novus Biological, NB100-2220), rabbit anti-p62 (1:1000), mouse anti-CTSD (1:100),mouse anti-GAPDH (1:10000; Sigma, G8795), rabbit anti-postsynaptic density 95 (PSD-95; 1:1000; Cell Signaling, 3409), and mouse anti-β-actin (1:800; Sigma, A2066). Immunopositive bands of horseradish peroxidase-conjugated secondary antibodies were detected with an ECL system (GE Healthcare) and exposure to ECL Hyperfilm.

2.12. Statistical analysis

The IBM SPSS statistics 25 (IBM, NY, USA) was used for statistical analysis. The normality of data distribution was assessed with the Kolmogorov-Smirnov test. For normally distributed variables, one-way analysis of variance (ANOVA) followed by the Bonferroni post hoc tests were used to assess differences between groups. The Kruskal–Wallis followed by Mann–Whitney *U* tests were used to explore differences between groups in non-normally distributed variables. Comparisons of beam-balance, beam-walking and Barnes maze latencies were made using two-way repeated measures ANOVA. Sample size calculation (power = 0.8, $\alpha = 0.05$) was performed using an online calculator (http://www.lasec.cuhk.edu.hk/sample-size-calculation.html). Estimated 5 animals per group would be required to detect ≥30% difference in brain tissue loss between the EPPS-treated and untreated groups with the 25% standard deviation of the mean value. Data were expressed as mean ± standard error of the mean (S.E.M.). Differences with $p < .05$ were considered statistically significant.

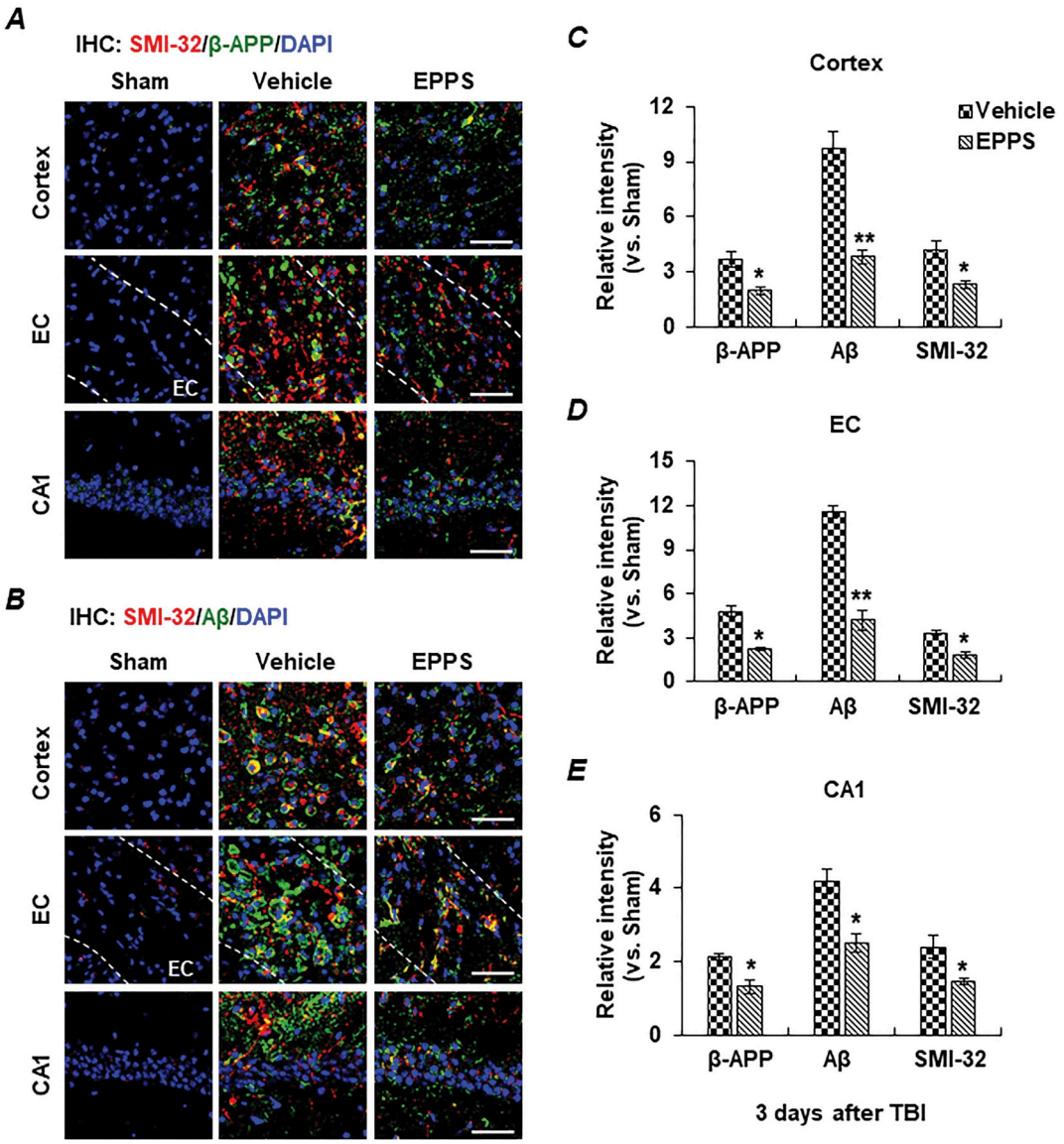

Fig. 2. EPPS treatment reduces β-APP and Aβ accumulation and SMI-32 expression at 3 days after TBI. Representative images of immunofluorescence staining showing (A) SMI-32 (red) and β-APP (green), and (B) SMI-32 (red) and Aβ (green). Images were taken from the pericontusional cortex, external capsule (EC), and hippocampal CA1 of the indicated groups. Semi-quantification of relative fluorescence intensity for β-APP, Aβ and SMI-32 in the pericontusional (C) cortex, (D) EC, and (E) hippocampal CA1 of the indicated groups. β-APP, beta-amyloid precursor protein; Aβ, beta-amyloid; SMI-32, nonphosphorylated neurofilament-H used as a marker of axonal damage. Scale bar = 50 μm. All data was expressed as mean ± S.E.M. and analyzed using the Kruskal-Wallis followed by Mann-Whitney *U* test. $n = 5$ mice per group. $^{*}p < .05$ and $^{**}p < .01$ vs. vehicle. (For interpretation of the references to colour in this figure legend, the reader is referred to the web version of this article.)

3. Results

3.1. EPPS treatment reduces beta-amyloid (Aβ) burden and axonal injury 3 days after TBI

It has been shown that TBI induces β-APP overexpression and Aβ accumulation which peaked at 1–3 days after injury in rodents (Ciallella et al., 2002; Loane et al., 2011). Immunohistochemistry showed that TBI induced marked accumulations of β-APP and Aβ along with increased expression of non-phosphorylated neurofilament-H (SMI-32, a marker of axonal damage) (Fig. 2A and B) over a widespread area detected in the pericontusional cortex (Fig. 2C), external capsule (EC, Fig. 2D), and hippocampal CA1 (Fig. 2E) of the vehicle-treated TBI mice. EPPS treatment significantly reduced TBI-induced β-APP and Aβ accumulations and SMI-32 expression in the above areas when compared with the vehicle-treated group.

3.2. EPPS treatment ameliorates neuronal autophagic flux and synaptic damage 3 days after TBI

Next, we determined the effect of EPPS treatment on the impairment of autophagic flux after TBI by assessing autophagosomal markers, microtubule-associated protein 1 light chain 3 (LC3) and p62/SQSTM1 (sequestosome 1). LC3 is widely used to monitor autophagy. During autophagy induction, the soluble form of LC3 (LC3-I) is converted to LC3-II, which is essential for autophagosome formation. The ratio of LC3-II to LC3-I (LC3-II/LC3-I) provides a metric for monitoring autophagy flux. p62 is an autophagy-specific substrate that is degraded through the autophagy–lysosomal pathway. The level of p62 is generally considered to correlate inversely with autophagic clearance (Koike et al., 2005). Western blot analysis showed that TBI significantly increased the LC3-II/LC3-I ratio and p62 protein level in the vehicle-treated group, and these effects were profoundly reduced in the EPPS-

treated group (Fig. 3A, B, and C). Moreover, western blot analysis revealed that TBI significantly reduced the level of postsynaptic density 95 (PSD-95), a potent regulator of excitatory postsynaptic strength, which was prevented by EPPS treatment (Fig. 3A and D). Furthermore, immunohistochemistry showed that TBI significantly increased the overall number of the p62-positive cells, as well as the number of the p62-positive neurons (marked by NeuN), over a widespread area detected in the pericontusional cortex (Fig. 3E and F) and hippocampal

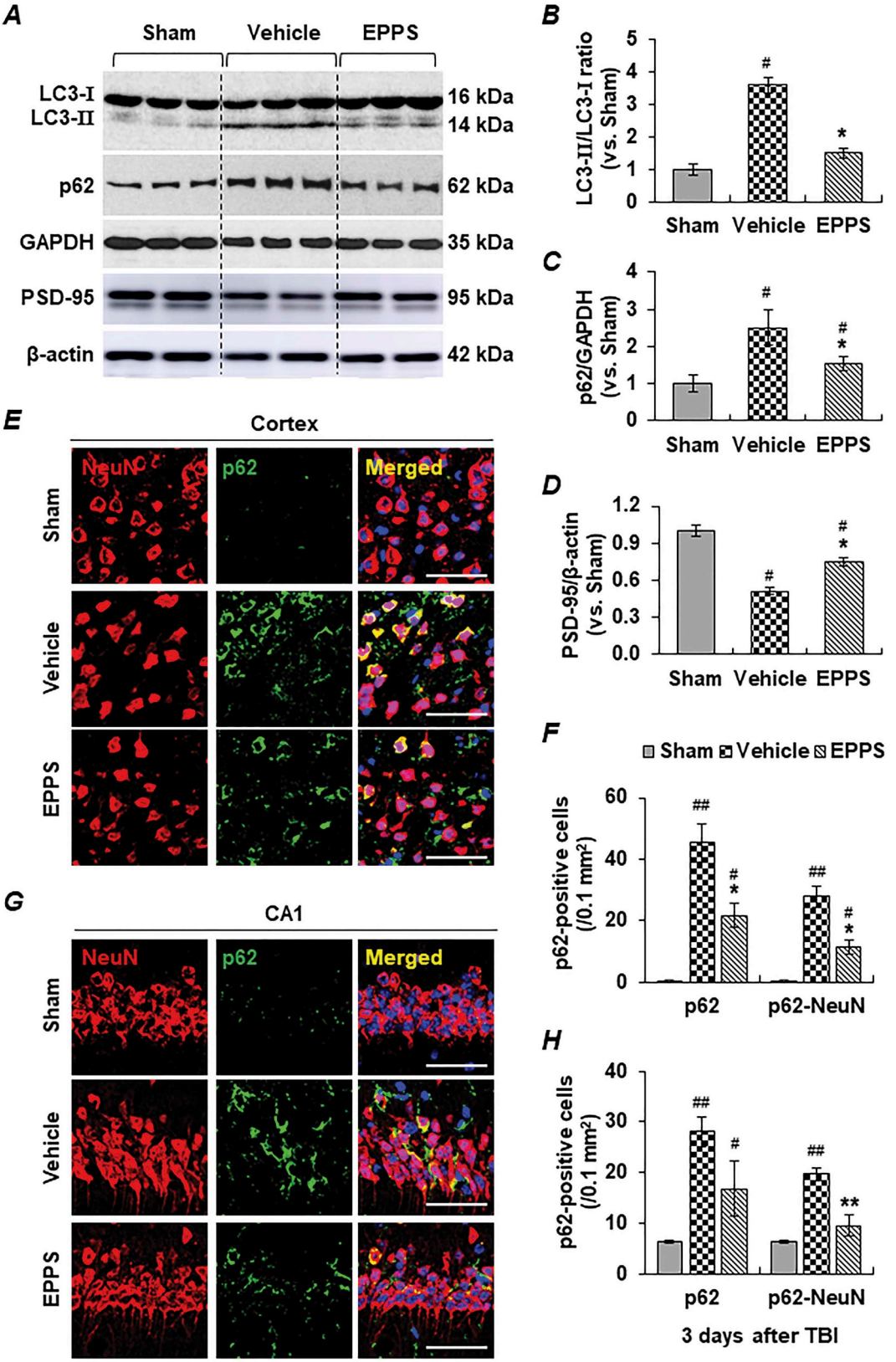

(caption on next page)

Fig. 3. EPPS treatment reduces neuronal autophagosome accumulation and synaptic damage at 3 days after TBI. (A) Representative images of Western blots showing the protein levels of autophagosomal markers, microtubule-associated protein 1 light chain 3 (LC3) and p62/SQSTM1 (sequestosome 1), as well as postsynaptic density 95 (PSD-95), in the injured cerebral cortex of the indicated groups. (B, C, D) Semi-quantitation of immunoblots was analyzed by densitometry, and data are expressed as the ratio of LC3-II to LC3-I (B), p62 level normalized to GAPDH (C), and PSD-95 level normalized to β-actin (D) from three independent experiments. (E, G) Representative images of immunofluorescence staining showing the expression and co-localization of the neuronal marker NeuN (red) and p62/SQSTM1 (green). Images were taken from the pericontusional (E) cortex and (G) hippocampal CA1 of the indicated groups. The number of overall p62-positive cells and p62-positive neurons in the pericontusional (F) cortex and (H) hippocampal CA1 were counted as described in the Methods section. Scale bar = 50 μm. All data was expressed as mean ± S.E.M. and analyzed using the Kruskal-Wallis followed by Mann-Whitney *U* test. $n = 5$ mice per group. $^{\#}p < .05$ and $^{\#\#}p < .01$ vs. sham and $^{*}p < .05$ and $^{**}p < .01$ vs. vehicle. (For interpretation of the references to colour in this figure legend, the reader is referred to the web version of this article.)

CA1 (Fig. 3G and H) in the vehicle-treated group, and these effects were profoundly reduced in the EPPS-treated group.

Lysosomal dysfunction is associated with early impairment of autophagic clearance after TBI (Sarkar et al., 2014). CTSD (cathepsin D) is a lysosomal enzyme that can be used as a marker to evaluate lysosomal function. Immunohistochemistry showed that the overall number of CTSD-positive cells as well as the number of CTSD-positive neurons increased in the vehicle-treated group compare with sham control, and further enhanced in the EPPS-treated group, as seen in the pericontusional cortex (Fig. 4A and B) and hippocampal CA1 (Fig. 4C and D). Western blot analysis revealed that the mature form of CTSD (30 kDa) was significantly increased in the EPPS-treated group when compared to vehicle-treated group (Fig. 4E and F), but the CTSD precursor protein (53 kDa) did not differ between two groups. In addition, the levels of CTSD were reduced at 1 day after TBI in both vehicle- and EPPS-treated groups when compared to sham control (Suppl. Fig. I), suggesting early impairment of lysosomal function induced by TBI. Taken together, our data suggest that EPPS treatment ameliorates the impairment of autophagy-lysosome pathway in neurons at 3 days after TBI.

3.3. EPPS treatment reduces autophagic neuronal cell death 3 days after TBI

Next, we determined the effect of EPPS treatment on autophagic cell death after TBI. TBI significantly increased the number of apoptotic neurons (marked by active caspase-3 staining) in the pericontusional cortex (Fig. 5A) and hippocampal CA1 (Fig. 5B) in the vehicle-treated group, and these effects were profoundly reduced in the EPPS-treated group (Fig. 5C). Similar results of apoptotic neurons were shown with TUNEL staining (Suppl. Fig. II). Moreover, the increased expression of p62/SQSTM1 (indicating impaired autophagic flux) almost exclusively co-localized with the increased expression of active caspase-3 in the pericontusional cortex (Fig. 5D and E), suggesting a role of impaired autophagic flux in neuronal death after TBI. Additionally, we found that in vivo inhibition of autophagic flux with chloroquine (CQ) by decreasing autophagosome-lysosome fusion significantly reversed the decreased expressions of p62/SQSTM1 (Fig. 6A, B and C) and A. casp3 (Fig. 6D, E and F) in neurons by EPPS treatment. Moreover, we demonstrated that CQ greatly abolished the suppressive effects of EPPS on TBI-induced depositions of β-APP (Suppl. Fig. III) and Aβ (Suppl. Fig. IV). Taken together, these results suggest that the neuroprotection by EPPS is, at least in part, related to improved autophagy flux.

3.4. EPPS treatment reduces contusion volumes and delayed damages to hippocampal neurons and white matter 28 days after TBI

Next, we examined the effect of EPPS treatment for the first 7 days on long-term brain damage after TBI. Treatment with EPPS significantly reduced the TBI-induced chronic neuronal loss in the hippocampal CA1 and CA3 (Fig. 7A and B), compared to the vehicle-treated group. Moreover, the treatment with EPPS significantly reduced white matter damage assessed by the LFB staining of myelin intensity in the EC (Fig. 7C and D). Overall, the contusion volume was reduced by 43.6% in the EPPS-treated group compared with the vehicle-treated group (Fig. 7E and F). These long-term protective effects are likely related to the EPPS-mediated reduction in chronic beta-amyloid burden. Immunohistochemistry showed that the short-term (7-day) EPPS treatment significantly reduced the accumulation of β-APP (Suppl. Fig. VA and VB) and Aβ (Suppl. Fig. VC and VD) over a widespread area at 28 days after TBI detected in the pericontusional cortex, external capsule (EC), and hippocampus (CA1 and CA3) compared with the vehicle-treated group.

3.5. EPPS treatment improves motor and cognitive functions after TBI

At last, we examined the effects of EPPS treatment on neurological functional outcomes. Rodents tend to have short-term spontaneous motor function recovery and develop somehow delayed but persisted hippocampus-dependent cognitive deficits following TBI (Chen et al., 2014; Hausser et al., 2018). Thus, we measured the motor function in the first 5 days and cognitive function at 24 to 28 days after TBI. In the motor function assessment (Fig. 8A), the beam-walking and beam-balance tests showed that EPPS-treated TBI mice performed significantly better than the vehicle-treated mice. In the cognitive function assessment (Fig. 8B), the Barnes maze test showed that EPPS-treated TBI mice significantly reduced the latency time (spatial learning) at 27 and 28 days after TBI and number of head-poke error made into incorrect holes (spatial memory) at 28 days after TBI, compared with the vehicle-treated mice. In addition, EPPS treatment improved the ability in discriminating novel object in the novel object recognition test at 28 days after TBI (Fig. 8C).

4. Discussion

The present study, for the first time, demonstrates that EPPS, newly discovered as inhibitor of beta-amyloid (Aβ), provides significant neuroprotection in experimental traumatic brain injury (TBI). Our results reveal two important neuroprotective mechanisms of EPPS against secondary neuronal and axonal injury following TBI. First, EPPS treatment reduces axonal injury-related beta-amyloid precursor protein (β-APP) and Aβ burden. Second, EPPS treatment ameliorates TBI-induced autophagic flux in neurons.

Clinical and experimental studies have shown close correlation between the depositions of Aβ and its precursor β-APP as a sign of secondary neuronal and axonal damage following TBI, resulting in serious impairment of the brain function and can sometimes be fatal (Ikonomovic et al., 2004; Scott et al., 2016). Although it is unclear whether the accumulation of β-APP in damaged axons after TBI serves a mechanistic role or is simply an epiphenomenon, β-APP has been implicated as a mechanism of Aβ burden in traumatic brain injury linked to the development of Alzheimer's disease (Johnson et al., 2010). β-APP can be sequentially cleaved by β- and γ-secretases to generate oligomeric neurotoxic forms of Aβ (Gatson et al., 2013). Aβ burden induces oxidative stress and neuroinflammation, leading to neuronal cell death and progressive neurological dysfunction after TBI (Mannix and Whalen, 2012). Treatments in reducing brain Aβ burden have been proven to be neuroprotective and beneficial in animal models of TBI (Shim and Stutzmann, 2016; Yu et al., 2012). Direct infusion of an anti-APP antibody into the damaged brain region has been shown to reduce brain tissue damage, neuronal degeneration and functional deficits after TBI in rats (Itoh et al., 2009). In the present study, we demonstrated that TBI induced abundant accumulations of β-APP and Aβ in

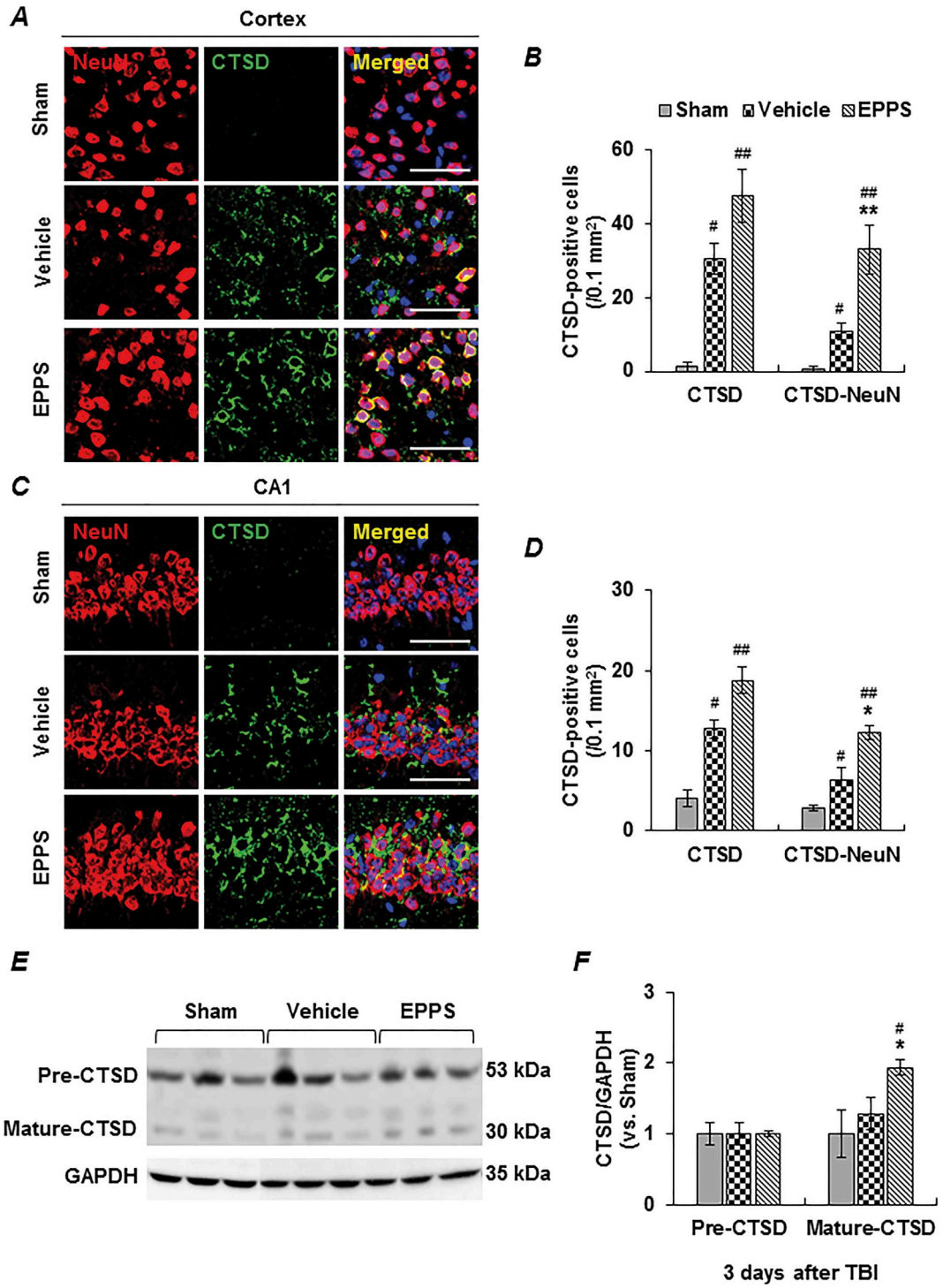

Fig. 4. EPPS treatment ameliorates the impairment of the autophagy-lysosome pathway in neurons at 3 days after TBI. (A, C) Representative images of immunofluorescence staining showing the expression and co-localization of the neuronal marker NeuN (red) and lysosomal enzyme cathepsin D (CTSD, green). Images were taken from the pericontusional (A) cortex and (C) hippocampal CA1 of the indicated groups. The number of overall CTSD-positive cells and CTSD-positive neurons in the pericontusional (C) cortex and (D) hippocampal CA1 were counted as described in the Methods section. Scale bar = 50 μm. (E) Representative images of Western blots showing the CTSD precursor form (53 kDa) and mature active form (30 kDa) in the injured cerebral cortex in the indicated groups. (F) Semi-quantitation of immunoblots was analyzed by densitometry. Data are expressed as fold changes of the two CTSD isoforms normalized to GAPDH (F) from three independent experiments. All data was expressed as mean ± S.E.M. and analyzed using the Kruskal-Wallis followed by Mann-Whitney U test. n = 5 mice per group. $^{\#}p < .05$ and $^{\#\#}p < .01$ vs. sham and $^{*}p < .05$ and $^{**}p < .01$ vs. vehicle. (For interpretation of the references to colour in this figure legend, the reader is referred to the web version of this article.)

the pericontusional cortex and the hippocampus (CA1) at 3 days after TBI, where SMI-32 (an indicator of axon damage) was highly co-expressed. Notably, EPPS treatment can simultaneously reduce β-APP, Aβ and SMI-32 in the above areas, which are associated with enhanced neuronal survival. While the primary tissue damage caused by TBI only directly affecting the cortical region of the brain, the TBI-induced

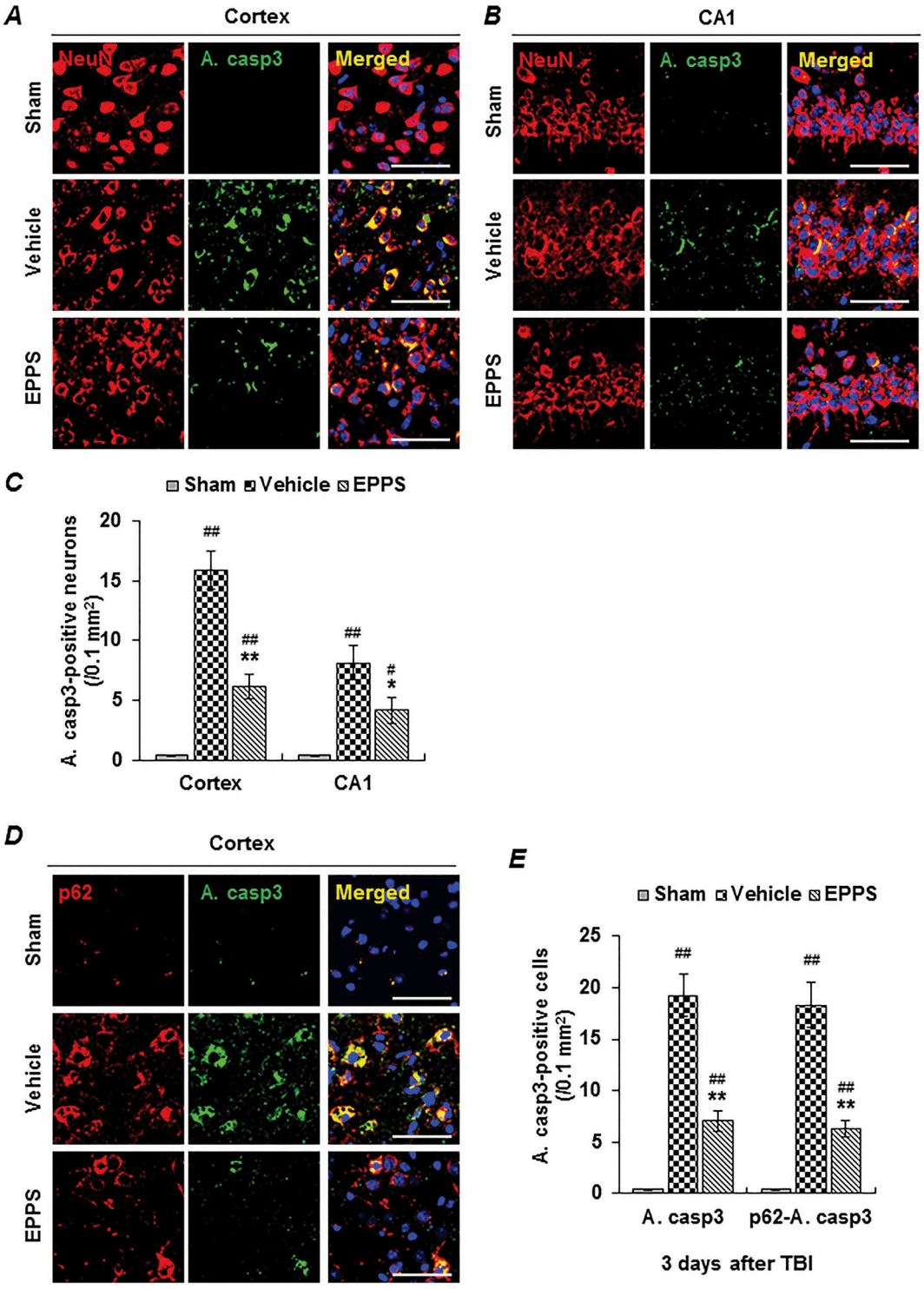

Fig. 5. EPPS treatment attenuates autophagic neuronal cell death at 3 days after TBI. (A, B) Representative images of immunofluorescence staining showing the expression and co-localization of the neuronal marker NeuN (red) and active caspase-3 (A. casp-3). Images were taken from the pericontusional (A) cortex and (B) hippocampal CA1 of the indicated groups. (C) The number of A. casp-3-positive neurons in the pericontusional cortex and hippocampal CA1 were counted as described in the Methods section. (D) Representative images of immunofluorescence staining showing the expression and co-localization of the autophagosomal marker p62/SQSTM1 (red) and active caspase-3 (A. casp-3, green) in the indicated groups. (E) The number of overall A. casp-3-positive cells and the p62 and A. casp-3 double-positive cells in the pericontusional cortex were counted as described in the Methods section. Scale bar = 50 μm. All data was expressed as mean ± S.E.M. and analyzed using the Kruskal-Wallis followed by Mann-Whitney U test. n = 5 mice per group. $^{\#}p < .05$ and $^{\#\#}p < .01$ vs. sham and $^{*}p < .05$ and $^{**}p < .01$ vs. vehicle. (For interpretation of the references to colour in this figure legend, the reader is referred to the web version of this article.)

accumulation of Aβ and β-APP as well as neuronal cell death were evidently detected throughout the pericontusional cortex and hippocampus of the mice in both acute (at 3 days) and chronic (at 28 days) stages of TBI. These results indicate an evolving cellular damage beyond the initial localized cortical damage induced by TBI. TBI often results in motor and cognitive impairments in patients and

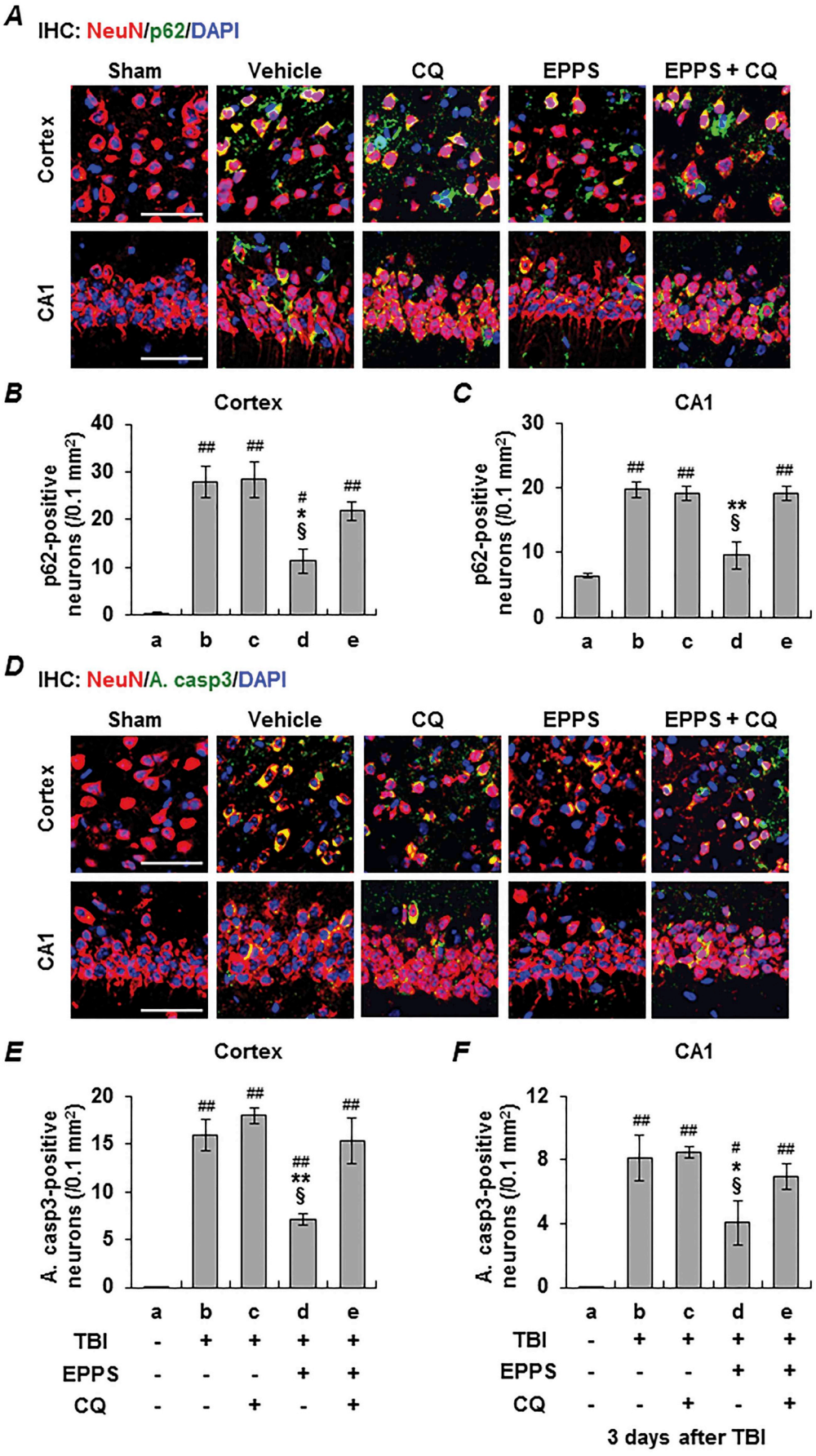

Fig. 6. Inhibition of autophagic flux with chloroquine (CQ) reverses the EPPS-induced decrease in autophagosome accumulation at 3 days after TBI. (A) Representative images of immunofluorescence staining showing the expression and co-localization of the neuronal marker NeuN (red) and autophagosomal marker p62/SQSTM1 (green) in the pericontusional cortex and hippocampal CA1 of the indicated groups. The number of p62-positive neurons in the pericontusional (B) cortex and (C) hippocampal CA1 were counted as described in the Methods section. Scale bar = 50 μm. All data was expressed as mean ± S.E.M. and analyzed using the Kruskal-Wallis followed by Mann-Whitney U test. $n = 4$ mice per group. $^{\#}p < .05$ and $^{\#\#}p < .01$ vs. sham, $^{*}p < .05$ and $^{**}p < .01$ vs. vehicle, and $^{\S}p < .05$ vs. EPPS + CQ. (For interpretation of the references to colour in this figure legend, the reader is referred to the web version of this article.)

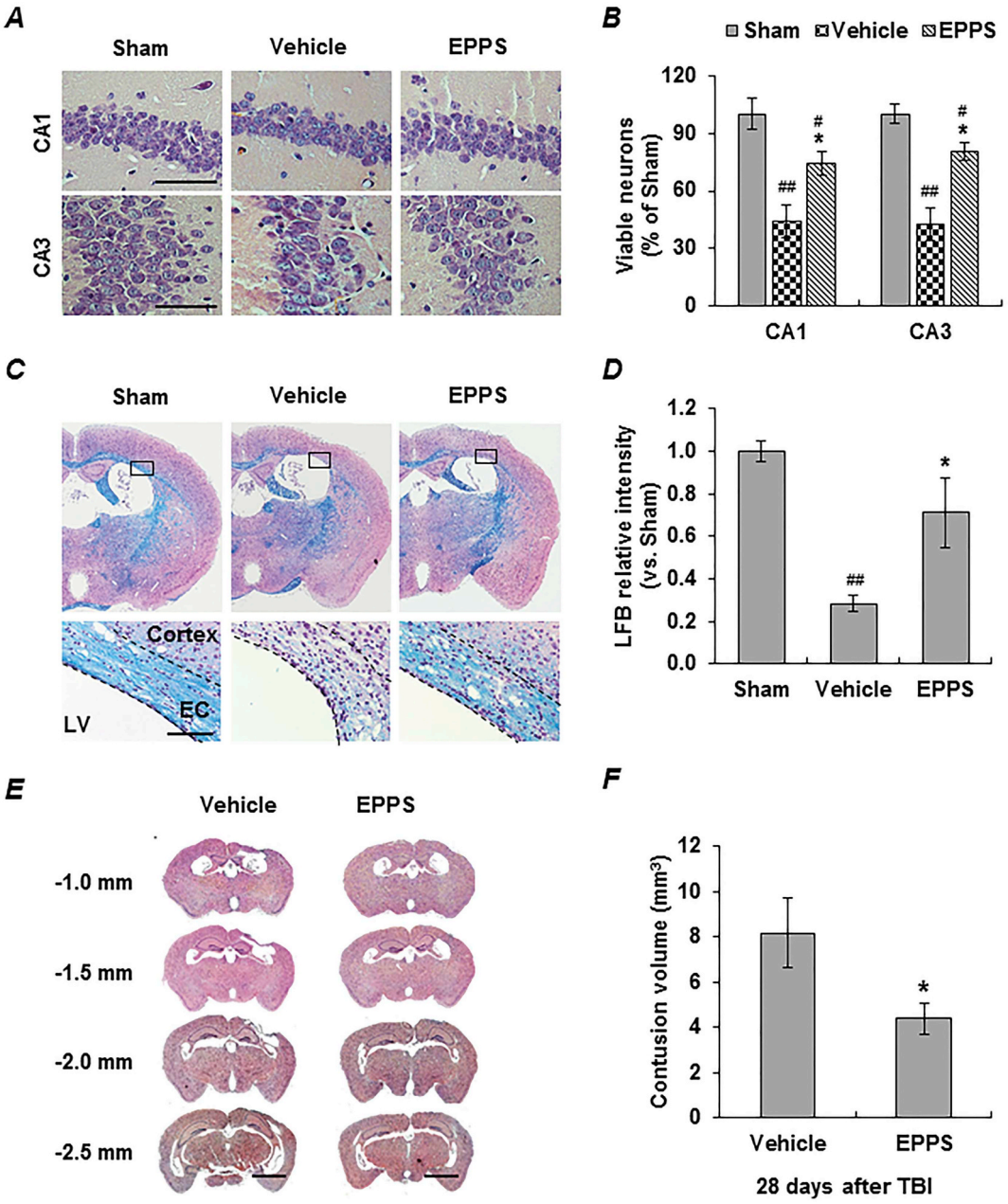

Fig. 7. EPPS treatment reduces damages to the hippocampus and white matter and contusion volumes at 28 days after TBI. (A) Representative H&E images showing the morphology of viable neurons in the hippocampal CA1 and CA3 in the indicated groups. Scale bar = 100 μm. (B) Quantification of the number of viable neurons in the indicated groups. (C) Representative Luxol fast blue (LFB) images of sham, vehicle- and EPPS-treated mice taken from ipsilateral hemisphere and external capsule (EC) for white matter integrity assessment. Scale bar = 100 μm. (D) Semi-quantification of relative LFB intensity in the EC of sham, vehicle- and EPPS-treated mice. $^{\#}p < .05$ and $^{\#\#}p < .01$ vs. sham and $^{*}p < .05$ vs. vehicle. (E) Representative H&E images showing whole brain coronal sections (−1.0, −1.5, −2.0 and − 2.5 mm relative to bregma) in the vehicle- and EPPS-treated mice. Scale bar = 1 mm. (F) The contusion volumes in vehicle- and EPPS-treated groups. All data was expressed as mean ± S.E.M. and analyzed using the Kruskal-Wallis followed by Mann-Whitney U test. n = 5 mice per group. $^{\#}p < .05$ and $^{\#\#}p < .01$ vs. sham and $^{*}p < .05$ vs. vehicle. (For interpretation of the references to colour in this figure legend, the reader is referred to the web version of this article.)

experimental animals associated with traumatic axonal injury (Hausser et al., 2018; Maas et al., 2008). Here, we show that early treatment with EPPS reduces the TBI-induced accumulation of Aβ and β-APP throughout the pericontusional cortex, hippocampus, and external capsule (white matter) in both the acute and chronic stages of TBI, resulting in improved cortex-dependent motor and hippocampus-dependent cognitive function following TBI.

Recent evidence implies that impaired autophagy flux may contribute to neuronal cell death after TBI. When autophagy is initiated, crescent-shaped double membrane structures form, which gradually elongate to enclose damaged macromolecules and organelles and eventually forms a double-membrane vesicle called autophagosome. This cargo-containing autophagosome then fuses with the lysosome to help degradation of its contents by lysosomal enzymes, a process termed as autophagic flux (Lipinski et al., 2015). Thus, impaired autophagic flux is characterized by reduced clearance of autophagosomes. When autophagic flux is impaired under pathological condition, autophagosomes containing toxic protein aggregates and defective organelles accumulate within the neurons, which may cause neurons to self-digestion and induce organellar stress and bioenergetics shortage in neurons. These, in turn, can trigger apoptotic or necrotic cell death (Maiuri et al., 2007). It has been shown that both autophagosomes and

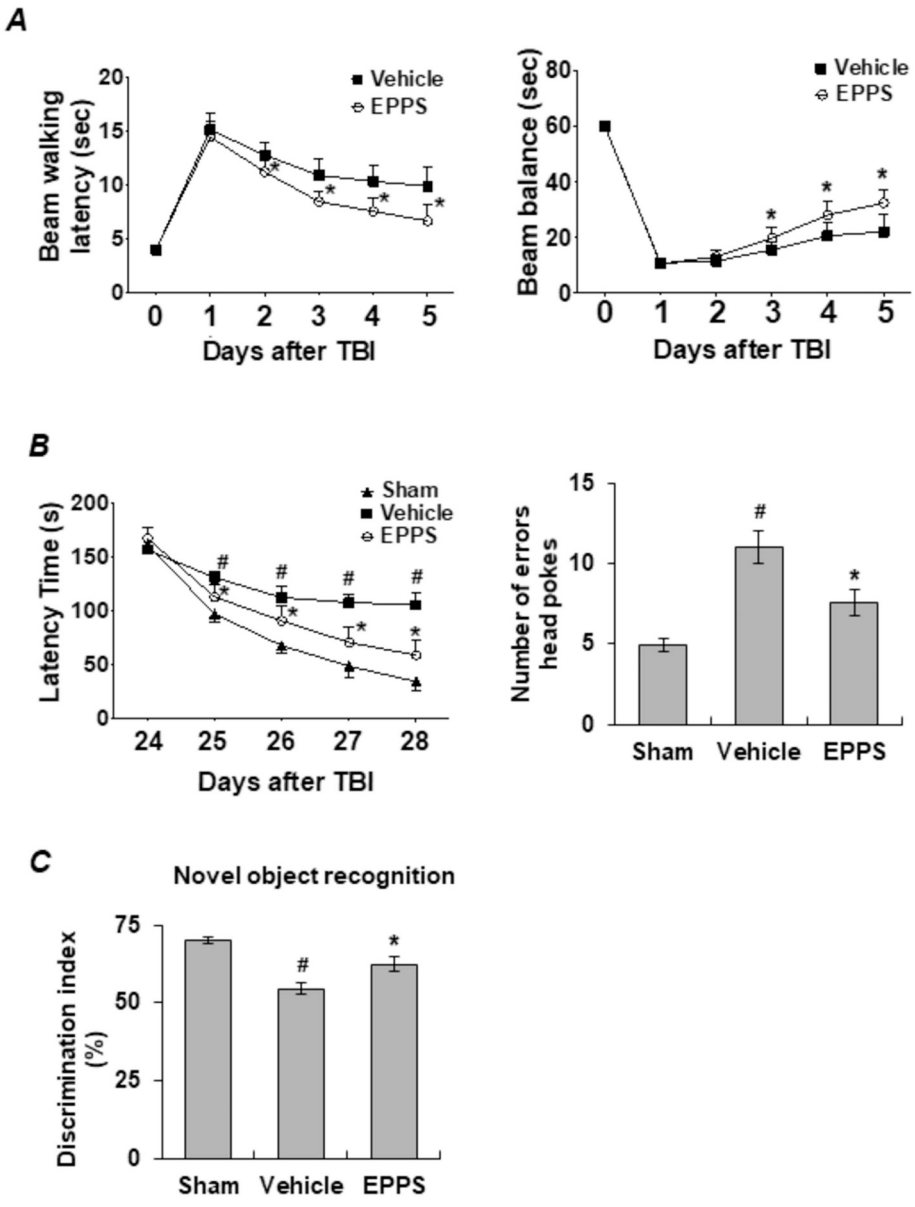

Fig. 8. EPPS treatment improves the short-term motor function and long-term cognitive function after TBI. (A) Beam walking (left) and beam balance (right) tests were conducted at 0 to 5 days after TBI to evaluate the motor function in vehicle- (close circle) and EPPS-treated (open circle) mice. (B) Barnes maze test was conducted at 24 to 28 days after TBI, and (C) novel object recognition was conducted at 28 days after TBI in sham, vehicle- and EPPS-treated mice. All data was expressed as mean ± S.E.M. Data for beam-balance, beam-walking and Barnes maze latencies were analyzed using two-way repeated measures analysis of variance (ANOVA). Data for number of errors head pokes and novel object recognition index were analyzed using one-way ANOVA followed by the Bonferroni post hoc tests. $n = 9$ mice per group. $^{\#}p < .05$ vs. sham and $^{*}p < .05$ vs. vehicle.

the autophagic substrate p62/SQSTM1 accumulated predominantly in neurons in the ipsilateral cortex and hippocampus immediately after TBI, and the increased p62/SQSTM1 peaked at day 1–3 but resolved by day 7 (Sarkar et al., 2014; Yin et al., 2017). The early impairment of autophagy is at least in part caused by lysosomal dysfunction, as evidenced by reduced protein levels and enzymatic activity of CTSD (cathepsin D). CTSD precursor protein (~53 kDa) can mature into active form (~30 kDa) in the lysosome and promotes autophagosome clearance (Gieselmann et al., 1983; Yogalingam and Pendergast, 2008). In the present study, we demonstrated that neuronal autophagy flux is impaired early after TBI due to lysosomal dysfunction and is associated with neuronal cell death, as evidenced by (1) activated autophagy as determined by increased expression of autophagy protein LC3-II, (2) reduced clearance of autophagosomes as determined by increased autophagic substrate p62/SQSTM1, and (3) strong colocalization of p62/SQSTM1 with activate caspase 3 (A. casp3, a marker of apoptotic cell death) in the neurons, detected in the ipsilateral cortex and the hippocampal CA1 region at 3 days after TBI. Enhancement of autophagic flux has been suggested to promote neuron survival in central nervous system (CNS) trauma (Zeng et al., 2018; Zhang et al., 2017). Our data indicate that EPPS treatment may accelerate the restoration of lysosomal dysfunction and enhance neuronal autophagic flux due to enhanced expression of mature CTSD, thereby increasing neuronal cell survival after TBI. Moreover, we found that inhibition of autophagic flux with chloroquine (CQ) by decreasing autophagosome-lysosome fusion (Mauthe et al., 2018), increased the neuronal p62 and A. casp3 expressions in EPPS-treated mice. Furthermore, we found that inhibition of autophagic flux with CQ significantly blocked the suppressive effect of EPPS treatment on axonal injury-associated β-APP and Aβ accumulations. These data suggest that the neuroprotective effect of EPPS is in part related to the restoration of autophagy flux.

It is well-recognized that accumulation of Aβ is associated with disruption of synaptic activity (Forner et al., 2017). Abnormal accumulation of autophagic vesicles has been reported to correlate with axonal and synaptic pathology in Alzheimer's disease (AD), and synaptic activity has been shown to enhance maturation of CTSD and autophagosomal-lysosomal degradation in neurons (Akwa et al., 2018; Sanchez-Varo et al., 2012). Autophagosomes was also detected in cell processes and axons in injured TBI brain (Clark et al., 2008), but the relationship between synaptic activity and autophagy after TBI is unknown. Postsynaptic density 95 (PSD-95) is a scaffold protein that is known to promote synapse maturation and to exert a major influence

on synaptic stability and glutamatergic neurotransmission in the brain. Notably, the loss of PSD-95 has shown to directly correlate with functional deficits after TBI (Wakade et al., 2010). Consistent with these observations, we detected PSD-95 was markedly reduced at a time point that paralleled with increased Aβ and autophagosomes accumulations and functional deficits after TBI, all of which was attenuated by EPPS treatment. These outcomes seem to indicate that there is a crosstalk between Aβ, synaptic activity and autophagy in the context of TBI, and support future therapeutic investigation by targeting this interplay to yield better outcomes after TBI.

In conclusion, our data provide new insights into neuroprotective mechanisms of EPPS in secondary neuronal and axonal injury after TBI by reducing brain Aβ burden and ameliorating neuronal autophagic flux.

Acknowledgement

This work was supported by the National Institutes of Health grants NS088719 and NS089991 (G.L.) and the Louisiana State University Health Sciences Foundation Fund for Schumpert Endowed Chair (G.L.).

Author disclosure statement

The authors declare that no competing financial interests exist.

Appendix A. Supplementary data

Supplementary data to this article can be found online at https://doi.org/10.1016/j.expneurol.2019.01.002.

References

Akwa, Y., Gondard, E., Mann, A., Capetillo-Zarate, E., Alberdi, E., Matute, C., Marty, S., Vaccari, T., Lozano, A.M., Baulieu, E.E., Tampellini, D., 2018. Synaptic activity protects against AD and FTD-like pathology via autophagic-lysosomal degradation. Mol. Psychiatry 23, 1530–1540.

Algattas, H., Huang, J.H., 2013. Traumatic brain injury pathophysiology and treatments: early, intermediate, and late phases post-injury. Int. J. Mol. Sci. 15, 309–341.

Au, A.K., Aneja, R.K., Bayir, H., Bell, M.J., Janesko-Feldman, K., Kochanek, P.M., Clark, R.S.B., 2017. Autophagy biomarkers Beclin 1 and p62 are increased in cerebrospinal fluid after traumatic brain injury. Neurocrit. Care. 26, 348–355.

Banerjee, R., Beal, M.F., Thomas, B., 2010. Autophagy in neurodegenerative disorders: pathogenic roles and therapeutic implications. Trends Neurosci. 33, 541–549.

Bilgen, M., 2005. A new device for experimental modeling of central nervous system injuries. Neurorehabil. Neural Repair 19, 219–226.

Button, R.W., Luo, S., 2017. The formation of autophagosomes during lysosomal defect: a new source of cytotoxicity. Autophagy 13, 1797–1798.

Chen, Y., Mao, H., Yang, K.H., Abel, T., Meaney, D.F., 2014. A modified controlled cortical impact technique to model mild traumatic brain injury mechanics in mice. Front. Neurol. 5, 100.

Choi, S.-H.H., Lee, D.Y., Kim, S.U., BK, Jin, 2005. Thrombin-induced oxidative stress contributes to the death of hippocampal neurons in vivo: Role of microglial nadph oxidase. J. Neurosci. 25, 4082–4090.

Ciallella, J.R., Ikonomovic, M.D., Paljug, W.R., Wilbur, Y.I., Dixon, C.E., Kochanek, P.M., Marion, D.W., DeKosky, S.T., 2002. Changes in expression of amyloid precursor protein and interleukin-1beta after experimental traumatic brain injury in rats. J. Neurotrauma 19, 1555–1567.

Clark, R.S., Bayir, H., Chu, C.T., Alber, S.M., Kochanek, P.M., Watkins, S.C., 2008. Autophagy is increased in mice after traumatic brain injury and is detectable in human brain after trauma and critical illness. Autophagy 4, 88–90.

Dash, P.K., Orsi, S.A., Zhang, M., Grill, R.J., Pati, S., Zhao, J., Moore, A.N., 2010. Valproate administered after traumatic brain injury provides neuroprotection and improves cognitive function in rats. PLoS One 5, e11383.

Faul, M., Xu, L., Wald, M.M., Coronado, V.G., 2010. Traumatic Brain Injury in the United States: Emergency Department Visits, Hospitalizations and Deaths 2002–2006, 2010 ed. Centers for Disease Control and Prevention, National Center for Injury Prevention and Control.

Forner, S., Baglietto-Vargas, D., Martini, A.C., Trujillo-Estrada, L., LaFerla, F.M., 2017. Synaptic impairment in alzheimer's disease: a dysregulated symphony. Trends Neurosci. 40, 347–357.

Gatson, J.W., Warren, V., Abdelfattah, K., Wolf, S., Hynan, L.S., Moore, C., Diaz-Arrastia, R., Minei, J.P., Madden, C., Wigginton, J.G., 2013. Detection of beta-amyloid oligomers as a predictor of neurological outcome after brain injury. J. Neurosurg. 118, 1336–1342.

Gieselmann, V., Pohlmann, R., Hasilik, A., Von Figura, K., 1983. Biosynthesis and transport of cathepsin D in cultured human fibroblasts. J. Cell Biol. 97, 1–5.

Hausser, N., Johnson, K., Parsley, M.A., Guptarak, J., Spratt, H., Sell, S.L., 2018. Detecting behavioral deficits in rats after traumatic brain injury. J. Vis. Exp.(131), 56044.

Ikonomovic, M.D., Uryu, K., Abrahamson, E.E., Ciallella, J.R., Trojanowski, J.Q., Lee, V.M., Clark, R.S., Marion, D.W., Wisniewski, S.R., DeKosky, S.T., 2004. Alzheimer's pathology in human temporal cortex surgically excised after severe brain injury. Exp. Neurol. 190, 192–203.

Itoh, T., Satou, T., Nishida, S., Tsubaki, M., Hashimoto, S., Ito, H., 2009. Improvement of cerebral function by anti-amyloid precursor protein antibody infusion after traumatic brain injury in rats. Mol. Cell. Biochem. 324, 191–199.

Jensen, E.C., 2013. Quantitative analysis of histological staining and fluorescence using ImageJ. Anat. Rec. (Hoboken) 296, 378–381.

Johnson, V.E., Stewart, W., Smith, D.H., 2010. Traumatic brain injury and amyloid-beta pathology: a link to Alzheimer's disease? Nat. Rev. Neurosci. 11, 361–370.

Kim, H.Y., Kim, H.V., Jo, S., Lee, C.J., Choi, S.Y., Kim, D.J., Kim, Y., 2015. EPPS rescues hippocampus-dependent cognitive deficits in APP/PS1 mice by disaggregation of amyloid-beta oligomers and plaques. Nat. Commun. 6, 8997.

Koike, M., Shibata, M., Waguri, S., Yoshimura, K., Tanida, I., Kominami, E., Gotow, T., Peters, C., von Figura, K., Mizushima, N., Saftig, P., Uchiyama, Y., 2005. Participation of autophagy in storage of lysosomes in neurons from mouse models of neuronal ceroid-lipofuscinoses (Batten disease). Am. J. Pathol. 167, 1713–1728.

Kumar, R., Husain, M., Gupta, R.K., Hasan, K.M., Haris, M., Agarwal, A.K., Pandey, C.M., Narayana, P.A., 2009. Serial changes in the white matter diffusion tensor imaging metrics in moderate traumatic brain injury and correlation with neuro-cognitive function. J. Neurotrauma 26, 481–495.

Laskowski, R.A., Creed, J.A., Raghupathi, R., 2015. Pathophysiology of mild TBI: implications for altered signaling pathways. In: Kobeissy, F.H. (Ed.), Brain Neurotrauma: Molecular, Neuropsychological, and Rehabilitation Aspects. CRC Press/Taylor & Francis(c) 2015 by Taylor & Francis Group, LLC., Boca Raton (FL).

Leger, M., Quiedeville, A., Bouet, V., Haelewyn, B., Boulouard, M., Schumann-Bard, P., Freret, T., 2013. Object recognition test in mice. Nat. Protoc. 8, 2531–2537.

Lipinski, M.M., Wu, J., Faden, A.I., Sarkar, C., 2015. Function and mechanisms of autophagy in brain and spinal cord trauma. Antioxid. Redox Signal. 23, 565–577.

Liu, C.L., Chen, S., Dietrich, D., Hu, B.R., 2008. Changes in autophagy after traumatic brain injury. J. Cereb. Blood Flow Metab. 28, 674–683.

Loane, D.J., Washington, P.M., Vardanian, L., Pocivavsek, A., Hoe, H.S., Duff, K.E., Cernak, I., Rebeck, G.W., Faden, A.I., Burns, M.P., 2011. Modulation of ABCA1 by an LXR agonist reduces beta-amyloid levels and improves outcome after traumatic brain injury. J. Neurotrauma 28, 225–236.

LoBue, C., Wadsworth, H., Wilmoth, K., Clem, M., Hart Jr., J., Womack, K.B., Didehbani, N., Lacritz, L.H., Rossetti, H.C., Cullum, C.M., 2017. Traumatic brain injury history is associated with earlier age of onset of Alzheimer disease. Clin. Neuropsychol. 31, 85–98.

Luong, T.N., Carlisle, H.J., Southwell, A., Patterson, P.H., 2011. Assessment of motor balance and coordination in mice using the balance beam. J. Vis. Exp. (49), 2376.

Maas, A.I., Stocchetti, N., Bullock, R., 2008. Moderate and severe traumatic brain injury in adults. Lancet Neurol. 7, 728–741.

Maiuri, M.C., Zalckvar, E., Kimchi, A., Kroemer, G., 2007. Self-eating and self-killing: crosstalk between autophagy and apoptosis. Nat. Rev. Mol. Cell Biol. 8, 741–752.

Mannix, R.C., Whalen, M.J., 2012. Traumatic brain injury, microglia, and beta amyloid. Int. J. Alzheimers Dis. 2012, 608732.

Mauthe, M., Orhon, I., Rocchi, C., Zhou, X., Luhr, M., Hijlkema, K.J., Coppes, R.P., Engedal, N., Mari, M., Reggiori, F., 2018. Chloroquine inhibits autophagic flux by decreasing autophagosome-lysosome fusion. Autophagy 14, 1435–1455.

Mondello, S., Buki, A., Barzo, P., Randall, J., Provuncher, G., Hanlon, D., Wilson, D., Kobeissy, F., Jeromin, A., 2014. CSF and plasma amyloid-beta temporal profiles and relationships with neurological status and mortality after severe traumatic brain injury. Sci. Rep. 4, 6446.

Patil, S.S., Sunyer, B., Hoger, H., Lubec, G., 2009. Evaluation of spatial memory of C57BL/6J and CD1 mice in the Barnes maze, the multiple T-maze and in the Morris water maze. Behav. Brain Res. 198, 58–68.

Piras, A., Collin, L., Gruninger, F., Graff, C., Ronnback, A., 2016. Autophagic and lysosomal defects in human tauopathies: analysis of post-mortem brain from patients with familial Alzheimer disease, corticobasal degeneration and progressive supranuclear palsy. Acta. Neuropathol. Commun. 4, 22.

Reichard, R.R., Smith, C., Graham, D.I., 2005. The significance of beta-APP immunoreactivity in forensic practice. Neuropathol. Appl. Neurobiol. 31, 304–313.

Roozenbeek, B., Maas, A.I., Menon, D.K., 2013. Changing patterns in the epidemiology of traumatic brain injury. Nat. Rev. Neurol. 9, 231–236.

Sanchez-Varo, R., Trujillo-Estrada, L., Sanchez-Mejias, E., Torres, M., Baglietto-Vargas, D., Moreno-Gonzalez, I., De Castro, V., Jimenez, S., Ruano, D., Vizuete, M., Davila, J.C., Garcia-Verdugo, J.M., Jimenez, A.J., Vitorica, J., Gutierrez, A., 2012. Abnormal accumulation of autophagic vesicles correlates with axonal and synaptic pathology in young Alzheimer's mice hippocampus. Acta Neuropathol. 123, 53–70.

Sarkar, C., Zhao, Z., Aungst, S., Sabirzhanov, B., Faden, A.I., Lipinski, M.M., 2014. Impaired autophagy flux is associated with neuronal cell death after traumatic brain injury. Autophagy 10, 2208–2222.

Scott, G., Ramlackhansingh, A.F., Edison, P., Hellyer, P., Cole, J., Veronese, M., Leech, R., Greenwood, R.J., Turkheimer, F.E., Gentleman, S.M., Heckemann, R.A., Matthews, P.M., Brooks, D.J., Sharp, D.J., 2016. Amyloid pathology and axonal injury after brain trauma. Neurology 86, 821–828.

Shim, S.S., Stutzmann, G.E., 2016. Inhibition of glycogen synthase kinase-3: an emerging target in the treatment of traumatic brain injury. J. Neurotrauma 33, 2065–2076.

Siebold, L., Obenaus, A., Goyal, R., 2018. Criteria to define mild, moderate, and severe traumatic brain injury in the mouse controlled cortical impact model. Exp. Neurol. 310, 48–57.

Wakade, C., Sukumari-Ramesh, S., Laird, M.D., Dhandapani, K.M., Vender, J.R., 2010.

Delayed reduction in hippocampal postsynaptic density protein-95 expression temporally correlates with cognitive dysfunction following controlled cortical impact in mice. J. Neurosurg. 113, 1195–1201.
Yin, Y., Li, E., Sun, G., Yan, H.Q., Foley, L.M., Andrzejczuk, L.A., Attarwala, I.Y., Hitchens, T.K., Kiselyov, K., Dixon, C.E., Sun, D., 2017. Effects of DHA on hippocampal autophagy and lysosome function after traumatic brain injury. Mol. Neurobiol. 55, 2454–2470.
Yogalingam, G., Pendergast, A.M., 2008. Abl kinases regulate autophagy by promoting the trafficking and function of lysosomal components. J. Biol. Chem. 283, 35941–35953.
Yu, F., Zhang, Y., Chuang, D.M., 2012. Lithium reduces BACE1 overexpression, beta amyloid accumulation, and spatial learning deficits in mice with traumatic brain injury. J. Neurotrauma 29, 2342–2351.
Zeng, X.J., Li, P., Ning, Y.L., Zhao, Y., Peng, Y., Yang, N., Zhao, Z.A., Chen, J.F., Zhou, Y.G., 2018. Impaired autophagic flux is associated with the severity of trauma and the role of A2AR in brain cells after traumatic brain injury. Cell Death Dis. 9, 252.
Zhang, M., Tao, W., Yuan, Z., Liu, Y., 2017. Mst-1 deficiency promotes post-traumatic spinal motor neuron survival via enhancement of autophagy flux. J. Neurochem. 143, 244–256.